Radiat Environ Biophys (2000) 39:265–273

ORIGINAL PAPER

Tomas Radivoyevitch

Time course solutions of the Sax-Markov binary eurejoining/misrejoining model of DNA double-strand breaks

Received: 23 December 1999 / Accepted: 1 July 2000

Abstract The Sax-Markov binary eurejoining/misrejoining (SMBE) model is a stochastic representation of Sax's breakage-and-reunion mechanism of misrejoining DNA double-strand breaks (DSBs). In this model, to approximate DSB misrejoining probabilities that decrease with increasing distance, the nucleus is treated as a collection of η isolated nuclear subvolumes called sites; DSB free ends within the same site interact with a probability that is independent of distance, and DSB free ends within different sites never interact. In our previous work, SMBE steady-state solutions were used to estimate η from a combination of high-dose PFGE (pulsed-field gel electrophoresis) data and moderate-dose chromosomal aberration data. Here, analytic SMBE transient solutions (i.e., time courses of DSBs and misrejoinings) are derived and used to estimate η from various sets of misrejoining DSB kinetic data. The time courses are multiexponentials with rate constants κ, 6κ, 15κ, ... $j(2j–1)\kappa$ corresponding to different nuclear site states and not different types of DSBs. For example, the κ component corresponds to nuclear sites with two DSB free ends and thus only one possible rejoining interaction, and the 6κ component corresponds to sites with four DSB free ends and thus six (four choose two) potential rejoining interactions – four of these six potential interactions lead to a final state of two misrejoinings and the other two of six lead to a final state of correct repair (unrejoinable DSBs are not represented in the SMBE model). The SMBE time course solutions provide site number estimates that fall in the range of $\eta \approx 10–100$ for premature chromosome condensation (PCC) data and $\eta \approx 1000$ for PFGE data.

T. Radivoyevitch (✉)
Department of Biometry and Epidemiology, 135 Rutledge Avenue, Medical University of South Carolina, Charleston, SC 29425, USA
e-mail: radivot@musc.edu
Tel.: +1 843 766 7064, Fax: +1 843 876 1126

Introduction

The Sax-Markov binary eurejoining/misrejoining (SMBE) model [1] is a stochastic representation of Sax's breakage-and-reunion mechanism of misrejoining DNA double-strand breaks (DSBs) [2]. It is a model that focuses exclusively on active DSBs with free ends that either eurejoin (rejoin correctly by chance) or misrejoin. The SMBE model, previously solved only in steady state [1], is solved here for all times. The solutions are time course predictions of DSBs and misrejoinings after acute doses of ionizing irradiation.

As an approximation to a model where DSB misrejoining probabilities decrease with increasing distance [3], the SMBE model treats the nucleus as a collection of η isolated nuclear subvolumes called sites [4]. DSB free ends within the same site interact with a probability that is independent of distance, and DSB free ends within different sites never interact. Steady-state SMBE solutions have been used to estimate the site number η from a combination of high-dose PFGE (pulsed-field gel electrophoresis) data [5] and moderate-dose chromosomal aberration data [6]; see [1]. The time course solutions derived here allow estimation of η from kinetic data.

The paper begins with brief reviews of the Sax subset (SS) [7] and SMBE [1] models, followed by a discussion of SS failure in the limit of low doses. Matrix exponentials and a flow graph approach are then used to find time courses for the simplest misrejoining SMBE subgraph, a five-state Markov model that approximates the SMBE model for doses low enough that complex misrejoinings (involving three or more breaks) are not created. The flow graph method is then extended to solve arbitrarily large finite SMBE subgraphs. The solutions in this case are multiexponentials with rate constants predicted to follow the sequence κ, 6κ, 15κ, ... $j(2j–1)\kappa$, where κ is an adjustable model parameter. The exponentials in this sequence correspond to different nuclear site states and not different types of DSBs. For example, the κ component corresponds to nuclear sites with two DSB free ends and thus only one possible rejoining interac-

tion, and the 6κ component corresponds to sites with four DSB free ends and thus six (four choose two) potential rejoining interactions – four of these six potential interactions lead to a final state of two misrejoinings and the other two lead to a final state of zero misrejoinings (unrejoinable DSBs are not modeled). The SMBE time course solutions are used to: (a) show that a deterministic equivalent of the SMBE model does not exist, and (b) form estimates of η from various sets of misrejoining DSB kinetic data.

Background

The SS model

Valid only in the limit of high doses because it ignores chance rejoining events of correct DSB free ends (i.e., eurejoining), the SS model [7] is

$$\frac{dU_1}{dt}(t) = -\lambda U_1(t) \qquad U_1(0) = (1-p)U(0) \tag{1}$$

$$\frac{dU_2}{dt}(t) = -\kappa_w U_2^2(t) \qquad U_2(0) = 2pU(0) \tag{2}$$

$$\frac{dM}{dt}(t) = \frac{1}{2}\kappa_w U_2^2(t) \qquad M(0) = 0 \tag{3}$$

with solutions

$$U_1(t) = U_1(0)e^{-\lambda s}, \quad U_2(t) = \frac{U_2(0)}{U_2(0)\kappa_w t + 1}$$

and

$$M(t) = \frac{U_2(0)}{2}\left(1 - \frac{1}{U_2(0)\kappa_w t + 1}\right).$$

Here, $U_1(t)$ is the per-cell average number of inactive DSBs – inactive DSBs can be thought of as "protein splinted" single entities that always repair correctly apart from some localized alterations in sequence; $U_2(t)$ is the per-cell average number of active DSB *free ends* – an active DSB is defined here as a pair of two DSB free ends not necessarily of the same origin; $M(t)$ is the average number of misrejoinings per cell – all active DSBs eventually misrejoin in the SS model; κ_w is the binary misrejoining rate constant for total active DSB free ends in the *whole* nucleus; p is the initial fraction of DSBs that are active to misrejoin; and $U(0)=GD$ is the initial number of all DSBs where $G\approx 40$ DSBs per Gy per human cell irradiated during the G_0/G_1 part of the cell cycle and D is the dose in Gy delivered acutely just before $t=0$. Please note that $U(t)=U_1(t)+(1/2)U_2(t)$ corresponds to the total number of DSBs at time t. The SS model is consistent with PFGE X-ray data (human fibroblasts; 80 Gy X-ray) [5] when $\lambda\approx 1.1$ per hour, $\kappa_w\approx 2.6\times 10^{-4}$ per hour and $P\approx 0.33$ [7].

The SS model was originally developed with the entire nucleus viewed as one well-mixed site. To obtain a per-site SS model we divide Eqs. 1–3 by the number of sites η and let $u_1(t)=U_1(t)/\eta$, $u_2(t)=U_2(t)/\eta$ and $m(t)=M(t)/\eta$ be the per-site average numbers of inactive DSBs, active DSB free ends and misrejoinings, respectively. The per-site SS model is then

$$\frac{du_1}{dt}(t) = -\lambda u_1(t) \qquad u_1(0) = \frac{U_1(0)}{\eta} \tag{4}$$

$$\frac{du_2}{dt}(t) = -\eta\kappa_w u_2^2(t) \qquad u_2(0) = \frac{U_2(0)}{\eta} \tag{5}$$

$$\frac{dm}{dt}(t) = \frac{1}{2}\eta\kappa_w u_2^2(t) \qquad m(0) = 0 \tag{6}$$

with solutions

$$u_1(t) = u_1(0)e^{-\lambda t} = \frac{U_1(0)}{\eta}e^{-\lambda t};$$

$$u_2(t) = \frac{u_2(0)}{u_2(0)\eta\kappa_w t + 1} = \frac{U_2(0)/\eta}{U_2(0)\kappa_w t + 1}$$

and

$$m(t) = \frac{u_2(0)}{2}\left(1 - \frac{1}{u_2(0)\eta\kappa_w t + 1}\right) = \frac{U_2(0)}{2\eta}\left(1 - \frac{1}{U_2(0)\kappa_w t + 1}\right).$$

In terms of averages for the whole cell these solutions become

$$U_1(t) = U_1(0)e^{-\lambda t}; \; U_2(t) = \frac{U_2(0)}{U_2(0)\kappa_w t + 1} = \frac{U_2(0)}{U_2(0)(\kappa/\eta)t + 1}$$

and

$$M(t) = \frac{U_2(0)}{2}\left(1 - \frac{1}{U_2(0)\kappa_w t + 1}\right) = \frac{U_2(0)}{2}\left(1 - \frac{1}{U_2(0)(\kappa/\eta)t + 1}\right)$$

where $\kappa=\eta\kappa_w$ is the per-site misrejoining rate constant; see Eqs. 5 and 6. Since the parameters κ and η appear in the solution only as the ratio $\kappa_w=\kappa/\eta$, individual estimates of κ and η are not possible using the SS model. The SMBE model allows estimation of η.

The SMBE model

The SMBE model [1] is a stochastic (Markov) extension of the SS model [7] that includes the accidental binary eurejoining of active DSB free ends. Other Markov models of misrejoining DSBs [8, 9] are stochastic extensions of a different classical kinetic model [10] corresponding to a Revell DSB misrejoining mechanism [11]. The SMBE model describes the dynamics of the probability that a nuclear site is in a specific state.

Let us define a nuclear site to be in state $\{j,i,m\}$ if it has j total active DSBs (i.e., pairs of DSB free ends), i active DSBs destined to misrejoin because their true mates have already misrejoined (these active DSBs are really two free ends of two separate DSBs), $j–i$ active DSBs still capable of eurejoining, and m misrejoinings. This state can undergo up to four types of transitions cor-

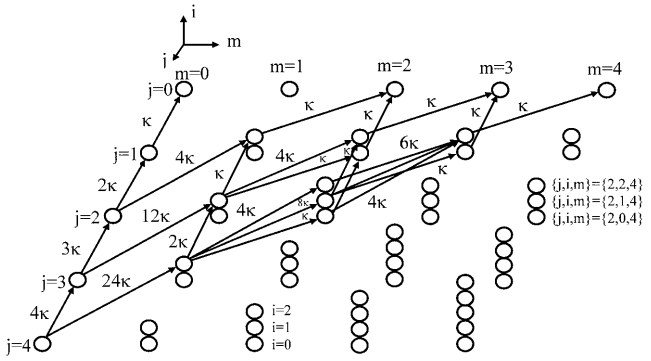

Fig. 1 The first few nodes (site states) of the SMBE model. A typical node {*j*,*i*,*m*} in this graph contains the probability mass at time *t* that a site has *j* active DSBs, *i* active DSBs destined to misrejoin, and *m* misrejoinings. The rate constants of probability mass transfer label the edges. As time evolves, the probability mass moves from the *j*-axis toward its final distribution on the *m*-axis

responding to four types of rejoining reactions: eurejoining within the *j*–*i* pool, misrejoining within the *j*–*i* pool, misrejoining within the *i* pool, and misrejoining between the *i* and *j*–*i* pools. For a site in state {*j*,*i*,*m*}, the rate constants of these four state transitions are $\kappa(j-i)$ to state {*j*–1,*i*,*m*}, $\kappa 2(j-i)(j-i-1)$ to state {*j*–1,*i*+1,*m*+1}, $\kappa i(2i-1)$ to state {*j*–1,*i*–1,*m*+1} and $\kappa 4i(j-i)$ to state {*j*–1,*i*,*m*+1}, each of these being κ times the number of potential free end interactions. The SMBE model can be viewed (Fig. 1) as a graph of nodes (site states) and arrows (state transitions) where a typical node {*j*,*i*,*m*} contains the probability mass $P(j,i,m;t)$ that a site is in state {*j*,*i*,*m*} at time *t*. Each node is also associated with a differential equation, e.g., at the node {2, 1, 1} we have

$$\frac{dP(2,1,1;t)}{dt} = 12\kappa P(3,0,0;t) + 2\kappa P(3,1,1;t) - (\kappa + 4\kappa + \kappa)P(2,1,1;t).$$

Thus, the graph of Fig. 1 is a linear system of coupled differential equations whose solution allows computation of the SMBE mean value time courses

$$u_a(t) = \sum_{m=0}^{\infty}\sum_{j=0}^{\infty}\sum_{i=0}^{\min(j,m)} jP(j,i,m;t)$$

and

$$m(t) = \sum_{m=0}^{\infty}\sum_{j=0}^{\infty}\sum_{i=0}^{\min(j,m)} mP(j,i,m;t).$$

The SMBE model does not treat inactive DSBs stochastically because they do not affect misrejoinings and because Poisson inactive DSBs remain Poisson under linear repair. The SS solution for the mean number of inactive DSBs can therefore be assumed when fitting the SMBE model to total DSB-rejoining data.

SS model failure

The SS model is inappropriate at low to moderate doses for several reasons discussed elsewhere [1, 7] including steady-state arguments against the SS misrejoining dose-response shape and magnitude, and kinetic arguments regarding the insensitivity of measured DSB-rejoining times to large increments in dose. An additional (though related) reason derives from the low-dose extreme situation where most sites have no active DSBs, and a negligible number of sites have more than one. In this situation, the SS mean number of active DSBs per cell is

$$U_a(t) = \frac{U_2(t)}{2} = \frac{U_a(0)}{U_a(0)2\kappa_w t + 1}$$

while, from Fig. 1, the SMBE mean number of active DSBs is

$$U_a(t) = \eta\frac{U_a(0)}{\eta}e^{-\kappa t}.$$

Thus, for a cell with just one active DSB, the SS model (with $\kappa_w \approx 2.6\times10^{-4}$ per hour [7]) suggests that the rejoining half-life will be $\tau_{1/2}=1/(2\kappa_w)\approx 80$ days, while, if $\eta\approx 400$ [1] so that $\kappa=\eta\kappa_w\approx 0.1$ per hour, the SMBE model suggests a much more realistic $\tau_{1/2}=\ln(2)/\kappa\approx 7$ h.

Time course solutions of the SMBE model

Matrix method

The 5-node SMBE subgraph in the left panel of Fig. 2, valid in the limit of moderate to low doses where misrejoinings involve fewer than three DSBs, is a linear system [12]

$$\frac{d}{dt}X(t) = \kappa AX(t) \quad \text{and} \quad Y(t) = CX(t)$$

where

$$A = \begin{pmatrix} 0 & 1 & 0 & 0 & 0 \\ 0 & -1 & 2 & 0 & 0 \\ 0 & 0 & -6 & 0 & 0 \\ 0 & 0 & 4 & -1 & 0 \\ 0 & 0 & 0 & 1 & 0 \end{pmatrix}, \quad C = \begin{pmatrix} 0 & 1 & 2 & 1 & 0 \\ 0 & 0 & 0 & 1 & 2 \end{pmatrix},$$

$$X(t) = \begin{pmatrix} x_1(t) \\ x_2(t) \\ x_3(t) \\ x_4(t) \\ x_5(t) \end{pmatrix} = \begin{pmatrix} P(0,0,0;t) \\ P(1,0,0;t) \\ P(2,0,0;t) \\ P(1,1,1;t) \\ P(0,0,2;t) \end{pmatrix}$$

and

$$Y(t) = \begin{pmatrix} u_a(t) \\ m(t) \end{pmatrix}.$$

The solution, written compactly using $e^{A\kappa t}=I+A\kappa t+A^2(\kappa t)^2/2+\ldots$, is

$$Y(t)=Ce^{A\kappa t}X(0)=Ce^{M\Lambda M^{-1}\kappa t}X(0)=CMe^{\Lambda\kappa t}M^{-1}X(0)$$

where Λ is the matrix of eigenvalues and M is the corresponding matrix of eigenvectors, i.e., $AM=M\Lambda$. The ini-

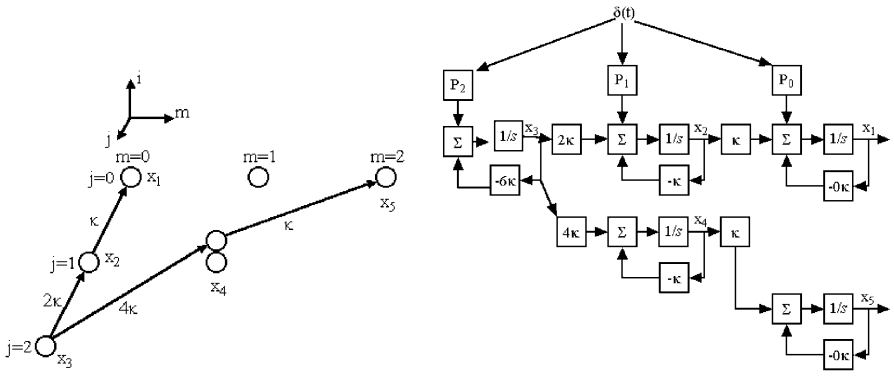

Fig. 2 The 5-node SMBE subgraph (*left panel*) and its corresponding block diagram (*right panel*). The outputs of the 1/*s* blocks (integrators) in the right panel are the state variables x_1 to x_5 of the left panel. The initial distribution of active DSBs is created by the Dirac delta function $\delta(t)$. Connections corresponding to the output matrix *C*, which maps the states into per-site average active DSBs and misrejoinings, are omitted for visual clarity

tial condition $X(0)=[P_0\ P_1\ P_2\ 0\ 0]'$ and the software MATLAB then yield

$$Y(t)=\begin{pmatrix}u_a(t)\\ m(t)\end{pmatrix}=\begin{pmatrix}0\\0\end{pmatrix}P_0+\begin{pmatrix}e^{-\kappa t}\\0\end{pmatrix}P_1 + \begin{pmatrix}1.2e^{-\kappa t}+0.8e^{-6\kappa t}\\ 1.3-0.8e^{-\kappa t}-0.53e^{-6\kappa t}\end{pmatrix}P_2.$$

Thus, in the limit of low doses, misrejoinings and active DSBs are expected to follow biexponential time courses with rate constants that differ by a factor of six.

Flow graph method

Laplace transforms [12, 13] will now be used in a flow graph approach to solving the 5-node SMBE model. This approach is extended to SMBE graphs of arbitrary size in the next section.

The 5-node SMBE subgraph can be represented by the block diagram shown in the right panel of Fig. 2. Here *s* is the Laplace variable, boxes labeled 1/*s* are integrators, and the outputs of the integrators are the state variables x_i. This system, equivalent to system 7 less the output relation $Y=CX$, corresponds to the matrix equation

$$\frac{d}{dt}X(t)=\kappa AX(t)+B\delta(t) \tag{8}$$

where $X(0^-)$ is a vector of zeros and $\delta(t)$ is a Dirac delta function, which, upon integration of Eq. 8 between $t=0^-$ (just before $t=0$) and $t=0^+$ (just after $t=0$) gives $X(0^+)=B=[P_0\ P_1\ P_2\ 0\ 0]'$ equal to the initial state of system 7. Thus, the 5-node SMBE autonomous system with nonzero initial conditions (Eq. 7) is now being viewed as a completely equivalent input driven system with zero initial conditions (Eq. 8), the input being the impulse function $\delta(t)$. This perspective is useful in the flow graph approach that follows.

Since SMBE subgraphs are linear systems, each state variable $x_i(t)$ can be decomposed into

$$x_i(t)=\sum_j x_{ij}(t)$$

where $x_{ij}(t)$ is the contribution to state x_i due to probability mass that traversed the input matrix element P_j. Beginning with P_0 and ending with P_2, we now consider each of these contributions.

Probability mass that traverses P_0 goes directly into x_1 and nowhere else, so $x_{i0}(t)=0$ for $i>1$. From Fig. 2 the Laplace transform of $x_{10}(t)$ is $\underline{x}_{10}(s)=P_0/s$. Thus $x_{10}(t)$ is a step function with height P_0. However, because $x_1(t)$ corresponds to site states with no active DSBs and no misrejoinings, it contributes nothing to the outputs and can therefore be ignored.

Probability mass that goes through P_1 contributes to $x_1(t)$ and $x_2(t)$. As mentioned above, only the latter of these is of interest. The Laplace transform of this contribution is $\underline{x}_{21}(s)=P_1/(s+\kappa)$, so $x_{21}(t)=P_1e^{-\kappa t}$. The state $x_2(t)$ contributes to $u_a(t)$ but not to $m(t)$.

Mass that traverses P_2 contributes to each of the five states. Again, we can ignore the path to x_1. The remaining four contributions are

$$\underline{x}_{32}(s)=\frac{P_2}{s+6\kappa},\qquad \underline{x}_{22}(s)=\left(\frac{P_2}{s+6\kappa}\right)\left(\frac{2\kappa}{s+\kappa}\right),$$

$$\underline{x}_{42}(s)=\left(\frac{P_2}{s+6\kappa}\right)\left(\frac{4\kappa}{s+\kappa}\right),\quad \underline{x}_{52}(s)=\left(\frac{P_2}{s+6\kappa}\right)\left(\frac{4\kappa}{s+\kappa}\right)\left(\frac{\kappa}{s}\right).$$

Mason's gain formula, a very practical tool for generating transfer functions by inspection [14], is useful here. For example, to get $\underline{x}_{32}(s)$, the product of the boxes along the forward path between $\delta(t)$ and x_3 (see Fig. 3) is divided by 1 minus the product of the boxes that lie in the loop that would be opened if the forward path were removed. The product of the forward path is $P_2(1/s)$ and the product of the loop factors is $-6\kappa(1/s)$ so

$$\underline{x}_{32}(s)=\frac{P_2(1/s)}{1-(-6\kappa)(1/s)}=\frac{P_2}{s+6\kappa}$$

To form the other transfer functions, we use the fact that the transfer function of two transfer functions in series is equal to the product of the transfer functions (note that multiplications in the Laplace domain correspond to convolutions in the time domain). Thus, since the path from x_3 to x_4 has a transfer function

$$\frac{4\kappa(1/s)}{1-(-\kappa)(1/s)}=\frac{4\kappa}{s+\kappa},$$

the overall transfer function to x_4 is the product

$$\underline{x}_{42}(s)=\left(\frac{P_2}{s+6\kappa}\right)\left(\frac{4\kappa}{s+\kappa}\right).$$

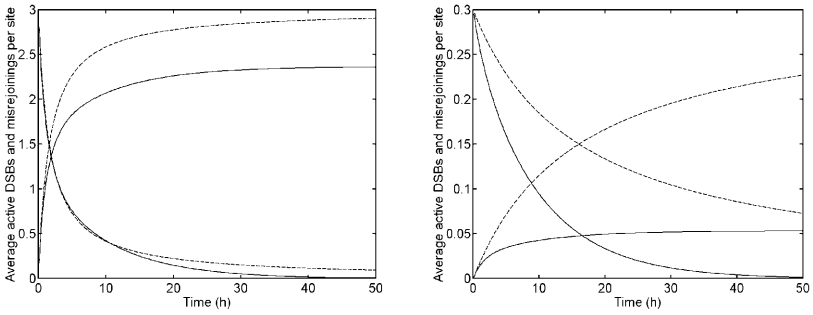

Fig. 3 A comparison of $u_a(t)$ and $m(t)$ for the SS (*dotted*) and SMBE (*solid*) models when κ=0.1 h^{-1}. *Left panel* For high doses [e.g., $u_a(0)$=3] the SS and SMBE models are similar except for eurejoining. *Right panel* For low to moderate doses [e.g., $u_a(0)$=0.3] the kinetics of the SS and SMBE solutions differ markedly. Throughout, an SMBE model of size J=10 is used with Poisson active DSBs at t=0

In this manner transfer functions to each of the states can be determined. Note that transfer functions to states corresponding to the same number of active DSBs, here $\underline{x}_{22}(s)$ and $\underline{x}_{42}(s)$, differ only by a constant in the numerator, so the corresponding time domain functions (the impulse responses) also differ by only a multiplicative constant. This fact is exploited extensively in an algorithm (below) that solves arbitrary-sized SMBE subgraphs.

To convert the Laplace domain solutions into time domain solutions we use partial fraction expansions. Since $\underline{x}_{32}(s)$ is already in its partial fractioned form, its inverse Laplace transform is, by inspection, $x_{32}(t)=P_2e^{-6\kappa t}$. To expand $\underline{x}_{22}(s)$, and thus also $x_{42}(s)=2\underline{x}_{22}(s)$, we write

$$\underline{x}_{22}(s)=\left(\frac{P_2}{s+6\kappa}\right)\left(\frac{2\kappa}{s+\kappa}\right)=\left(\frac{A_1}{s+6\kappa}\right)+\left(\frac{A_2}{s+\kappa}\right)$$

and find the residues A_1 and A_2 using the formula $A_k=(s-p_k)\underline{x}_{22}(s)|_{s=p_k}$ where p_k is the kth pole,

$$A_1=P_2\left(\frac{2\kappa}{-6\kappa+\kappa}\right)=-P_2(2/5)$$

and

$$A_2=2\kappa\left(\frac{P_2}{-\kappa+6\kappa}\right)=P_2(2/5).$$

Thus,

$$x_{22}(t)=-P_2(2/5)e^{-6\kappa t}+P_2(2/5)e^{-\kappa t}$$

and

$$x_{42}(t)=-P_2(4/5)e^{-6\kappa t}+P_2(4/5)e^{-\kappa t}$$

Our last task is to partial fraction

$$\underline{x}_{52}(s)=\left(\frac{P_2}{s+6\kappa}\right)\left(\frac{2\kappa}{s+\kappa}\right)\left(\frac{\kappa}{s}\right)$$
$$=\left(\frac{A_1}{s+6\kappa}\right)+\left(\frac{A_2}{s+\kappa}\right)+\left(\frac{A_3}{s}\right).$$

The residues in this case are $A_1=P_2(4/30)$, $A_2=-P_2(4/5)$, and $A_3=P_2(4/6)$, so

$$x_{52}(t)=P_2((2/3)-(4/5)e^{-\kappa t}+(4/30)e^{-6\kappa t}).$$

Putting this all together we have

$$u_a(t)=2x_{32}(t)+x_{42}(t)+x_{22}(t)+x_{21}(t)$$
$$=P_2(4/5)e^{-6\kappa t}+P_2(6/5)e^{-\kappa t}+P_1e^{-\kappa t}$$

and

$$m(t)=2x_{52}(t)+x_{42}(t)$$
$$=P_2((4/3)-(4/5)e^{-\kappa t}-(16/30)e^{-6\kappa t})$$

in complete agreement with the matrix method result given earlier.

Arbitrary-sized SMBE subgraphs

Let us define an SMBE subgraph of size J as the set of all nodes and arrows reachable from $\{J,0,0\}$. Thus, the model J=2 has 5 nodes, the model J=3 has 10 nodes, and the model J=4 has 18 nodes; see Fig. 1. How large should J be to adequately approximate the SMBE model? If the distribution of active DSBs per site is initially Poisson with mean $u_a(0)$ less than 4, over 99% of the probability mass will remain within an SMBE subgraph of size J=10. The data sets analyzed in this paper all yield $u_a(0)<2$, so the model J=10 should be adequate. In general, a model is sufficiently large if extensions to higher J values do not lead to noticeable changes in the solutions.

To solve SMBE subgraphs of arbitrary size J we will construct matrices K_u and K_m such that

$$u_a(t)=P'K_uE \text{ and } m(t)=P'K_mE \quad (9)$$

where E is the column vector $[1\ e^{-\kappa t}\ e^{-6\kappa t}\ ...\ e^{-J(2J-1)\kappa t}]'$ and P' is the row vector $[P_0\ P_1\ P_2\ ...\ P_J]$. Here, the first two rows of K_u and K_m, with P and E truncated accordingly, solve the SMBE model of size J=1, the first three rows solve the model J=2, ... and the first J+1 rows (i.e., the full matrices) solve the model of size J. In the algorithm described below, the rows are constructed independently of one another. It therefore suffices to consider the algorithm for just one row.

Suppose we wish to build the (J+1)th row of K_u and K_m. The first step is to compute partial fraction expansions for a basis set of J+1 Laplace transforms $1/[(s+J(2J\text{-}1)\kappa)...(s+j'(2j'\text{-}1)\kappa)]$ where j' ranges between 0 and J. For example, the basis set for the third row of the K matrices is $1/(s+6\kappa)$, $1/[(s+6\kappa)(s+\kappa)]$ and $1/[(s+6\kappa)(s+\kappa)s]$. The partial fraction expansions

$$\prod_{j=j'}^{J}\frac{1}{s+j(2j-1)\kappa}=\sum_{j=j'}^{J}\frac{A_j}{s+j(2j-1)\kappa}$$

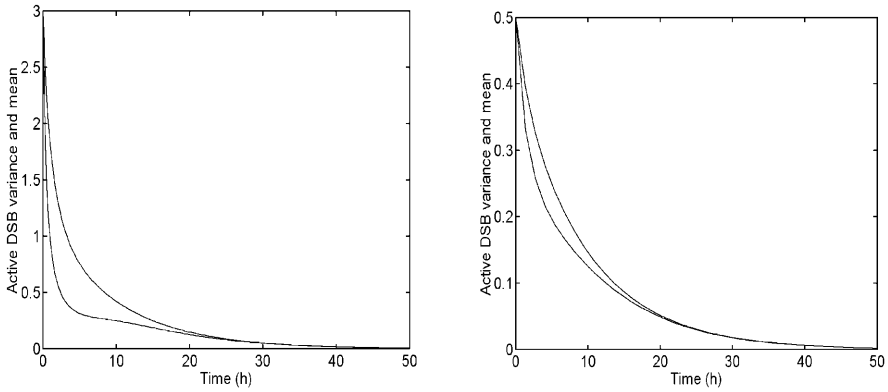

Fig. 4 The variance (*lower curve*) and mean (*upper curve*) of the per-site active DSB distribution. Initially Poisson with means of 3 (*left panel*) and 0.5 (*right panel*), the distribution of active DSBs per site becomes underdispersed due to binary reaction kinetics. As the mean falls well below one the distribution resumes a unit dispersion

have trivial inverse Laplace transforms

$$\sum_{j=j'}^{J} A_j e^{-j(2j-1)\kappa t}.$$

Thus, computing the residues

$$A_k = \prod_{j=j\neq k'}^{J} \frac{1}{-k(2k-1)\kappa + j(2j-1)\kappa}$$

is equivalent to taking inverse Laplace transforms. The residues for each of the basis functions are computed and stored in an array. (Note that the set of basis functions will differ for each row of the K matrices.)

In the next part of the algorithm, the (J+1)th row of K_u (or K_m) is found by summing over all states x_k={j',i',m'}, the product of j' (or m'), the vector of residues for j' from step one above, and the numerator of the Laplace transform $\underline{x}_{kJ}(s)$. How do we visit all the states and how do we compute the numerator of $\underline{x}_{kJ}(s)$? The numerator of $\underline{x}_{kJ}(s)$ is the product of all rate constants that lie between {J,0,0} and {j',i',m'}. Thus, we can start at {J,0,0} and a numerator of 1, and we can push the rate constants forward to the next nodes as cumulative products. Before each push, the numerator at that node is used to compute the corresponding contributions to the (J+1)th rows of the K matrices. The sequence of pushes and node visitations is taken directly from the steady-state SMBE algorithm [1]. An implementation of this algorithm in Matlab is available upon request from the author, *radivot@musc.edu*. The case J=5 gives

$$K_u = \begin{pmatrix} 0 & 0 & 0 & 0 & 0 & 0 \\ 0 & 1.0000 & 0 & 0 & 0 & 0 \\ 0 & 1.2000 & 0.8000 & 0 & 0 & 0 \\ 0 & 1.2857 & 1.3333 & 0.3810 & 0 & 0 \\ 0 & 1.3333 & 1.6970 & 0.8205 & 0.1492 & 0 \\ 0 & 1.3636 & 1.9580 & 1.2308 & 0.3949 & 0.0527 \end{pmatrix}$$

and

$$K_m = \begin{pmatrix} 0 & 0 & 0 & 0 & 0 & 0 \\ 0 & 0 & 0 & 0 & 0 & 0 \\ 1.333 & -0.800 & -0.533 & 0 & 0 & 0 \\ 2.400 & -1.029 & -1.067 & 0.305 & 0 & 0 \\ 3.429 & -1.143 & -1.455 & 0.703 & 0.128 & 0 \\ 4.444 & -1.212 & -1.741 & 1.094 & 0.351 & -0.047 \end{pmatrix}.$$

Applying matrices like these (but with J=10) to Eq. 9 with $P_j = e^{-u} a^{(0)} u^j{}_a(0)/j!$ gives the plots shown in Fig. 3. From these plots, and from the equations above, it can be seen that, as dose increases, so too does the contribution of faster exponentials. In this manner the SMBE solution emulates the SS solution; the SS-rejoining rate increases with dose because $u_a(0)$ multiplies κ. Note also from these plots that, aside from differences in $m(t)$ due to the absence of accidental binary eurejoining in the SS model, the SS and SMBE solutions become increasingly similar as doses increase.

Higher moments

The SMBE mean values $m(t)$ and $u_a(t)$ were solved by the flow graph method in the previous section. In this section, our interest is in the time course of the variance of the active DSB distribution. This time course, obtained by applying matrix methods to the SMBE model collapsed onto its j-axis, is compared to $u_a(t)$ in Fig. 4. Active DSBs are seen here to become underdispersed quite rapidly, returning to normal dispersion only after the mean has become much less than one. Underdispersion results because the SMBE rate constants increase supralinearly as $\kappa j(2j-1) > \kappa j$. Had the rate constants been κj, corresponding to a classical kinetic rejoining equation that was linear in the mean number of active DSBs, the initial Poisson distribution would have remained Poisson as it regressed toward the origin. Instead, since we have binary reaction kinetics, the upper tail of the distribution is driven toward the origin faster than for linear kinetics, so underdispersion results. At later times, as $u_a(t)$ approaches zero, $P(0) \approx 1 - u_a(t)$ and $P(1) \approx u_a(t)$ so the variance $u_a(t) - u_a{}^2(t)$ approaches the mean $u_a(t)$.

When forming classical kinetic equations for the mean values of random variables (e.g., the SS model) it is often necessary to make assumptions about higher moments. Typical assumptions include neglecting the variance relative to the mean, or assuming that it equals the mean. Though such assumptions may be valid for certain systems in certain operating regimes, there will be situations where the assumptions break down. A comparison of the plots in Fig. 4 indicates that the variance of active DSBs depends on more than just the mean. In particular,

a mean of 0.5 corresponds to a variance less than 0.5 in the left panel and a variance equal to 0.5 in the right panel. Thus, for dosing situations where the variance cannot be neglected relative to the mean, since the variance cannot be reexpressed as a function of the mean, classical kinetic (mean value) models with solutions identical to the mean value time courses of the SMBE model are not likely to be found.

Comparison to experimental data

Using nonlinear least squares, SMBE time course solutions were fit to PFGE data (human fibroblasts; 80 Gy X-ray) [5] as shown in Fig. 5. The fit yielded an estimate of $\eta \approx 1000$ nuclear sites. This estimate is substantially higher than those obtained in the remainder of this section using various sets of PCC (premature chromosome condensation) data.

In PCC experiments using FISH (fluorescence in situ hybridization), it is possible to measure time courses for total, incomplete, reciprocal, and complex misrejoinings [15, 16], as well as time courses for the percentage of misrejoined cells with one, two, or more misrejoinings [17]. How can we create SMBE outputs that *approximate* these quantities? Consider the 5-node system $J=2$ shown in Fig. 2. In this system $\eta f\ 2x_5(t)=r(t)$ and $\eta f\ x_4(t)=i(t)$ are the expected number of reciprocal and incomplete exchange misrejoinings per cell, respectively, where $f=2.05(1-g)g$ and g is the painted fraction of the genome [18]. For complex aberrations $c(t)$, larger graphs are required. In Fig. 1, let $i(t)$ equal ηf times the probability mass in all nodes defined by $m=1$, let $r(t)$ equal ηf times twice the probability mass in the two nodes defined by $\{j<2, i=0, m=2\}$, and let $c(t)$ equal ηf times the m-weighted sum of the probabilities in all the other nodes – note that $c(t)$ includes some reciprocal and incomplete exchanges, so these are merely approximations. Matrices K_i, K_r and K_c generated in a manner similar to K_m, then yield

$$i(t)=\eta f\, P' K_i\, E,\ r(t)=\eta f\, P' K_r\, E, \text{ and } c(t)=\eta f\, P' K_c\, E.$$

Similarly, the percentages of misrejoined cells with one, two, or more misrejoinings can be obtained from analogously defined matrices K_1, K_2 and K_3. Together, these model outputs allow estimation of the SMBE model parameters from PCC time course data.

A simultaneous fit of the SMBE model to the time course data (human fibroblasts; 10 Gy gamma-rays) in Figs. 1 and 3 of Brown et al. [17] gave the plots in Fig. 6 and gave the estimate $\eta \approx 10$. One interpretation of the model's failure for $t>20$ h is that active DSBs can become unrejoinable with time, and complex misrejoinings tend to require diffusion distances and rejoining times that are larger than for reciprocal exchanges. Thus, some of the probability mass that the SMBE model transfers to complex misrejoinings should really be transferred to a trapping state (corresponding to unrejoinable DSBs not in the SMBE model) indistinguishable from incomplete exchanges ($m=1$ misrejoinings).

In modeling PCC lymphocyte data [15, 16] a problem arises in that a substantial number of misrejoinings appear "instantaneously" after the 20-min chromosome condensation period. In the present form of the SMBE model, misrejoinings cannot rise rapidly, plateau, and then rise again later with slower kinetics. Thus, consistent with the modeling assumptions of Wu et al. [19], a constant misrejoining offset has been added to $r(t)$ in the left panel of Fig. 7 and to each of $i(t)$, $r(t)$ and $c(t)$ in the right panel of Fig. 7. From these figures we see that the SMBE model fails for complex aberrations. The data

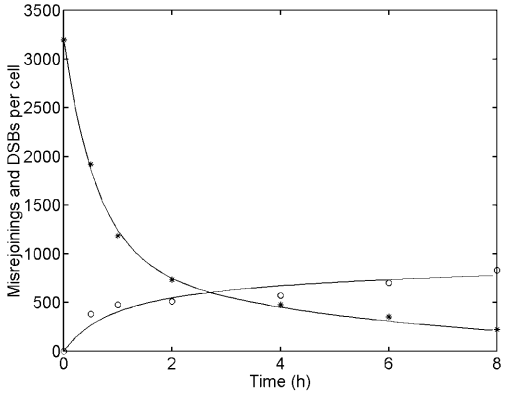

Fig. 5 Total DSBs (*) and total misrejoinings (o) for human fibroblast (80 Gy X-ray) PFGE data [5]. Parameter estimates from the SMBE time course fit are $u_a(0)=1.4$, $\kappa=0.18$, $\eta=1000$, $\lambda=1.7$ and $p=0.47$. Data points in all figures were taken visually from the publications

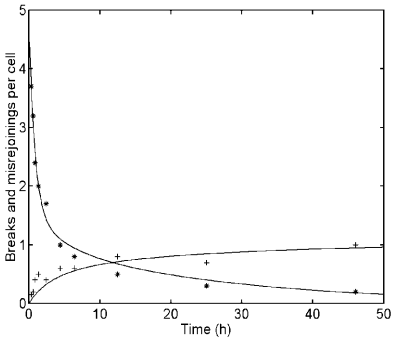

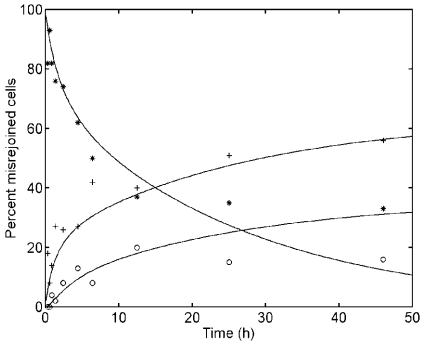

Fig. 6 Human fibroblast (10 Gy gamma-ray) PCC data [17]. The SMBE model was fit to data in both panels simultaneously. *Left panel* Time courses for total breaks (∗) and misrejoinings (+). *Right panel* The percentage of misrejoined cells with one misrejoining (∗), with two misrejoinings (+), and with more than two misrejoinings (o). The parameter estimates were $u_a(0)=1.5$, $\kappa=0.04$, $\eta=9.7$, $\lambda=1.3$ and $p=0.36$

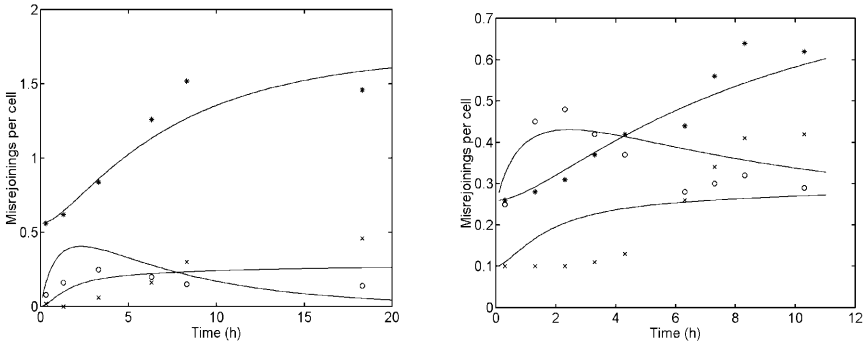

Fig. 7 Human lymphocyte PCC data [15, 16]. Here incomplete (○), reciprocal (∗) and complex (×) misrejoinings are plotted with their respective SMBE model outputs $i(t)$, $r(t)$ and $c(t)$, respectively. The parameter estimates were $u_a(0)=0.5$, $\kappa=0.14$, $\eta=83$ in the left panel (7 Gy, gamma-rays) and $u_a(0)=0.76$, $\kappa=0.11$, $\eta=8$ in the right panel (5 Gy, carbon ions)

seem to suggest that DSBs destined to become complex misrejoinings slowly migrate into neighboring sites where other active DSBs are more likely to be on other chromosomes. The site number estimates are $\eta\approx83$ (left panel; human lymphocytes; 7 Gy gamma-rays) and $\eta\approx8$ (right panel; human lymphocytes; 5 Gy carbon ions).

Greinert et al. [20] published PCC time course data for dicentrics and excess fragments in human lymphocytes irradiated with 4 Gy of X-rays. Using a misrejoining offset as before, subtracting the final unrejoined breaks from the excess fragment data, and replacing the first four dicentric values by artificial values that go to zero as $t=0$, an SMBE estimate of $\eta\approx66$ was obtained.

Thus, to summarize the results of this section, SMBE site number estimates seem to lie in the range of $\eta\approx10$–100 for PCC data and $\eta\approx1000$ for PFGE data.

Discussion

Why does η differ between experiments? Different cell types, LETs, assays, laboratories and failure of the SMBE modeling assumptions are all plausible reasons.

Is there any evidence for the (κ, 6κ, 15κ, ...) SMBE hypothesis? For CHO cells in G_0/G_1, active DSB-rejoining time constants inferred from dicentric yields in delayed plating ($\tau\approx75$ min) and split dose ($\tau\approx11$ min) experiments [21] lend some support to at least the (κ, 6κ) part of the SMBE hypothesis, but other data using G_2 human fibroblasts [22] are less supportive ($\tau\approx90$ and $\tau\approx5$ min). Wu et al. [19] modeled PCC data with the rate-determining step in DSB rejoining placed downstream of the broken end collision. Wu's model predicts that total misrejoinings follow a single exponential and that the misrejoining subcomponents $i(t)$, $r(t)$ and $c(t)$ follow a (κ, 2κ) hypothesis. Wu's model seems to fit the PCC data as well as the SMBE model.

It has been observed that differences in LET lead to differences in unrejoinable breaks at large times, but little differences in time constants [16, 23]. These observations are consistent with the SMBE model – SMBE rate constants do not depend on the initial distribution of active DSBs.

In systems theory, a state variable is nonmeasureable but observable if its time course can be estimated from its influence on the dynamics of other quantities that are measurable [12]. For example, active and inactive DSBs are observable but nonmeasureable when the SS model [7] is fit to PFGE data [5]. In fitting the SMBE model to PCC data, it was implicitly assumed that nonmeasurable $PFGE^+PCC^-$ breaks and misrejoinings do not alter the dynamics of measurable PCC^+ breaks and misrejoinings. If this is not the case, $PFGE^+PCC^-$ quantities should be included in models that are fit to PCC data, for they may be observable. However, since it is likely that $PFGE^+PCC^-$ quantities operate on a smaller distance scale ($\eta\approx1000$) than the PCC^+ quantities ($\eta\approx10$–100), the model would then need some modifications. For example, perhaps slow passage of PCC^+ quantities can be allowed between neighboring sites, or perhaps big sites can be defined as clusters of interacting little sites.

Acknowledgements I thank Prof. R.K. Sachs and the reviewers for their suggestions. This publication is supported in part by funds from NIH GM57245-03, the U.S. Department of Energy cooperative agreement DE-FC02-98CH10902, and by DOE grant DE-FG02-99ER62728.

Appendix

The following MATLAB program computes K matrices for arbitrary-sized SMBE graphs:

```
JVAL=10; % JVAL is the J value of the SMBE subgraph
Ku=zeros(JVAL, JVAL+1); Km=zeros (JVAL, JVAL+1);
Ki=zeros(JVAL, JVAL+1); Kr=zeros (JVAL, JVAL+1);
Kc=zeros (JVAL, JVAL+1);
for n=1:JVAL, %n is the row index for the K matrices
% Part I: compute the residue basis set
 a=1:n;
 a=a.*(2*a–1);% a is the vector of 2j choose 2 kappa coefficients
 RES=[]; % initialize RES as an empty matrix
 for j=n:–1:1, % start at the back of the flow graph and come in
A=poly(–a(j:n)); % convert root form to power form
  [r p]=residue(1, A); % get the residues, 1=numerator, A=denom
  res=[zeros(1, j) fliplr(r')];
  RES=[RES; res];
 end %Note that the products of kappa's cancel out
 A=poly(–[0 a]); % now do the last row in RES, i.e., j=0
 [r p]=residue (1, A);
 res=[fliplr(r')];
 RES=[RES; res];
% Part II: use the residue basis set and SMBE graph to find
% u_a(t) and m(t) given that the site contains exactly n actives.
 UT=n*RES(1,:); MT=0*res; % initialize the running totals
 IT=0*res; %incomplete
 RT=0*res; %reciprocal
 CT=0*res; %complex
```

```
M=[zeros (1, n) 1]; % start with 1 in the nth node
for m=1:(n+1),
 nM=zeros (m+1, n+1); % stack at the next m value
 for J=(n+1):–1:2,
  I=1;
  while (I<=m)&(I<=J),
   i=I–1; % i and j are the math indices
   j=J–1; % I and J are the matrix indices
   nm1=(j–i); % (eurejoin: eu within hopefuls)
   nm2=2*(j–i)*(j–i–1); %(mis within hopefuls)
   nm3=i*(2*i–1); %(mis within destined)
   nm4=4*(j–i)*i; %(mis between hopefuls and destineds)
    M(I, J–1)=M(I, J–1)+nm1*M(I, J);
    UT=UT+(j–1)*M(I, J–1)*RES(n+2–j,:);
   MT=MT+(m–1)*M(I, J–1)*RES(n+2–j,:);
   if ((m–1)==1) IT=IT+(m–1)*M(I, J–1)*RES(n+2–j,:);
   elseif ((m–1)==2)&((j–1)<2)&(i==0)
    RT=RT+(m–1)*M(I, J–1)*RES(n+2–j,:);
   else CT=CT+(m–1)*M(I, J–1)*RES(n+2–j,:);
   end
    nM(I, J–1)=nM(I, J–1)+nm4*M(I, J); % now do pushes to the
   nM(I+1, J–1)=nM(I+1, J–1)+nm2*M(I, J); % nM stack
   if i>0,
    nM(I–1, J–1)=nM(I–1, J–1)+nm3*M(I, J);
   end;
  M(I, J)=0;
  I=I+1;
  end; % while loop on I and i
 end; % for loop on J and j
 M=nM; %next M starts with what was pushed onto it
end % m loop
Ku(n, 1:(n+1))=UT; Km(n, 1:(n+1))=MT;
Ki(n, 1:(n+1))=IT; Kr(n, 1:(n+1))=RT; Kc(n, 1:(n+1))=CT;
end% n loop
```

References

1. Radivoyevitch T, Hoel DG, Chen AM, Sachs RK (1998) Misrejoining of double-strand breaks after X irradiation: relating moderate to very high doses by a Markov model. Radiat Res 149:59–67
2. Sax K (1940) An analysis of X-ray induced chromosomal aberrations in *Tradescantia*. Genetics 25:41–68
3. Kellerer AM, Rossi HH (1978) A generalized formulation of dual radiation action. Radiat Res 75:471–488
4. Kellerer AM, Rossi HH (1972) The theory of dual radiation action. Curr Top Radiat Res Q 8:85–158
5. Lobrich M, Rydberg B, Cooper PK (1995) Repair of x-ray-induced DNA double-strand breaks in specific Not I restriction fragments in human fibroblasts: joining of correct and incorrect ends. Proc Natl Acad Sci U S A 92:12050–12054
6. Lloyd DC, Edwards AA (1983) Chromosome aberrations in human lymphocytes: effect of radiation quality, dose, and dose rate. In: Ishihara T, Sasaki M (eds) Radiation-induced chromosome damage in man. Liss, New York
7. Radivoyevitch T, Hoel DG, Hahnfeldt PJ, Rydberg B, Sachs RK (1998) Recent data obtained by pulsed-field gel electrophoresis suggest two types of double-strand breaks. Radiat Res 149:52–58
8. Albright N (1989) A Markov formulation of the repair-misrepair model of cell survival. Radiat Res 118:1–20
9. Sachs RK, Chen PL, Hahnfeldt PJ, Hlatky LR (1992) DNA damage caused by ionizing radiation. Math Biosci 112:271–303
10. Tobias CA (1985) The repair-misrepair model in radiobiology: comparison to other models. Radiat Res Suppl 8:S77–S95
11. Revell SH (1974) The breakage-and-reunion theory and the exchange theory for chromosomal aberrations induced by ionizing radiations: a short history. In: Lett J, Adler H, Zelle M (eds) Adv Radiat Biol. Academic Press, New York
12. Kailath T (1980) Linear systems. Prentice-Hall, Englewood Cliffs, NJ
13. Oppenheim AV, Willsky AS, Young IT (1983) Signals and Systems. Prentice Hall, Englewood Cliffs, NJ
14. Philips CL, Nagle HT (1990) Digital control system analysis and design. Prentice Hall, Englewood Cliffs, NJ
15. Durante M, George K, Wu H, Yang TC (1996) Rejoining and misrejoining of radiation-induced chromatin breaks. I. Experiments with human lymphocytes. Radiat Res 145:274–280
16. Durante M, Furusawa Y, George K, Gialanella G, Greco O, Grossi G, Matsufuji N, Pugliese M, Yang TC (1998) Rejoining and misrejoining of radiation-induced chromatin breaks. IV. Charged particles. Radiat Res 149:446–454
17. Brown JM, Evans JW, Kovacs MS (1993) Mechanism of chromosome exchange formation in human fibroblasts: insights from “chromosome painting”. Environ Mol Mutagen 22:218–224
18. Lucas JN, Awa A, Straume T, Poggensee M, Kodama Y, Nakano M, Ohtaki K, Weier HU, Pinkel D, Gray J (1992) Rapid translocation frequency analysis in humans decades after exposure to ionizing radiation. Int J Radiat Biol 62:53–63
19. Wu H, Durante M, George K, Goodwin EH, Yang TC (1996) Rejoining and misrejoining of radiation-induced chromatin breaks. II. Biophysical model. Radiat Res 145:281–288
20. Greinert R, Detzler E, Volkmer B, Harder D (1995) Kinetics of the formation of chromosome aberrations in X-irradiated human lymphocytes: analysis by premature chromosome condensation with delayed fusion. Radiat Res 144:190–197
21. Greinert R, Volkmer B, Virsik-Peuckert RP, Harder D (1996) Comparative study of the repair kinetics of chromosomal aberrations and DNA strand breaks in proliferating and quiescent CHO cells [published erratum appears in Int J Radiat Biol 1997 Feb;71(2):231]. Int J Radiat Biol 70:33–43
22. Gotoh E, Kawata T, Durante M (1999) Chromatid break rejoining and exchange aberration formation following gamma-ray exposure: analysis in G2 human fibroblasts by chemically induced premature chromosome condensation. Int J Radiat Biol 75:1129–1135
23. Loucas BD, Geard CR (1994) Kinetics of chromosome rejoining in normal human fibroblasts after exposure to low- and high-LET radiations. Radiat Res 138:352–360